APPENDIX B

SUPPLEMENT TO CHAPTER 3

This appendix provides supplementary material for Chapter 3. Data that is summarized in Chapter 3, but not presented for brevity is presented here. Please reference Chapter 3 for terminology, methods, and complete results.

B.1 Position Reporting

CCV, k_s, and E_{vib} data records from multiple bi-directional passes over test beds with wood beams (loosened trench for E_{vib} data) are presented in Figures B.1 through B.3. Results are summarized in Chapter 3.

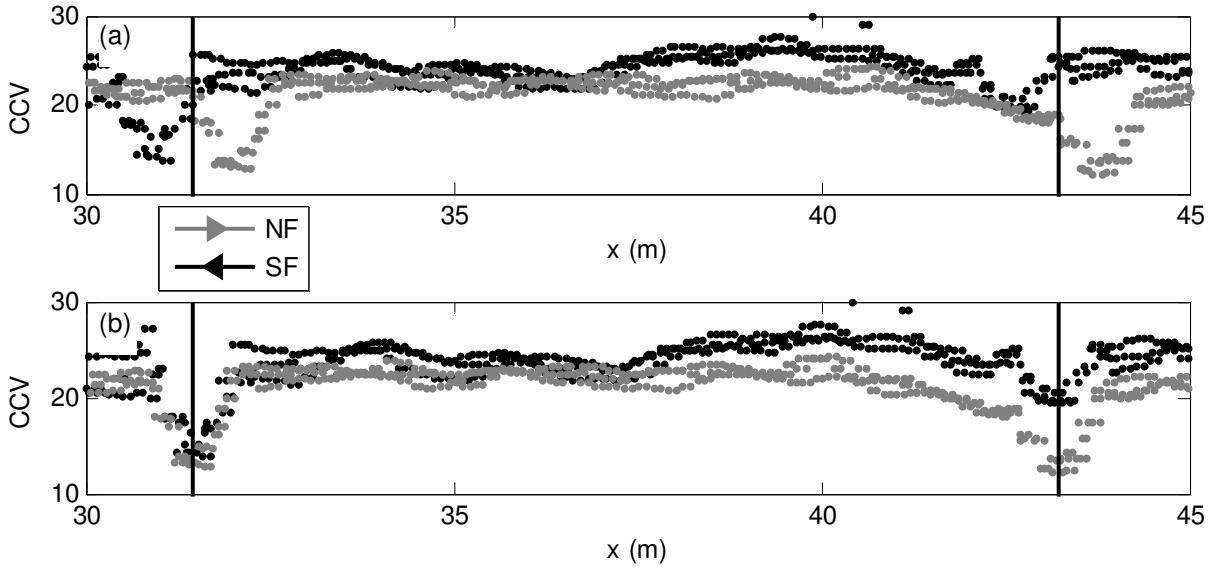

Figure B.1: Position error observed in CCV data records (TBFL12): (a) observed MV records with no position correction; (b) MV position corrected by -0.55 m (1.8 ft)

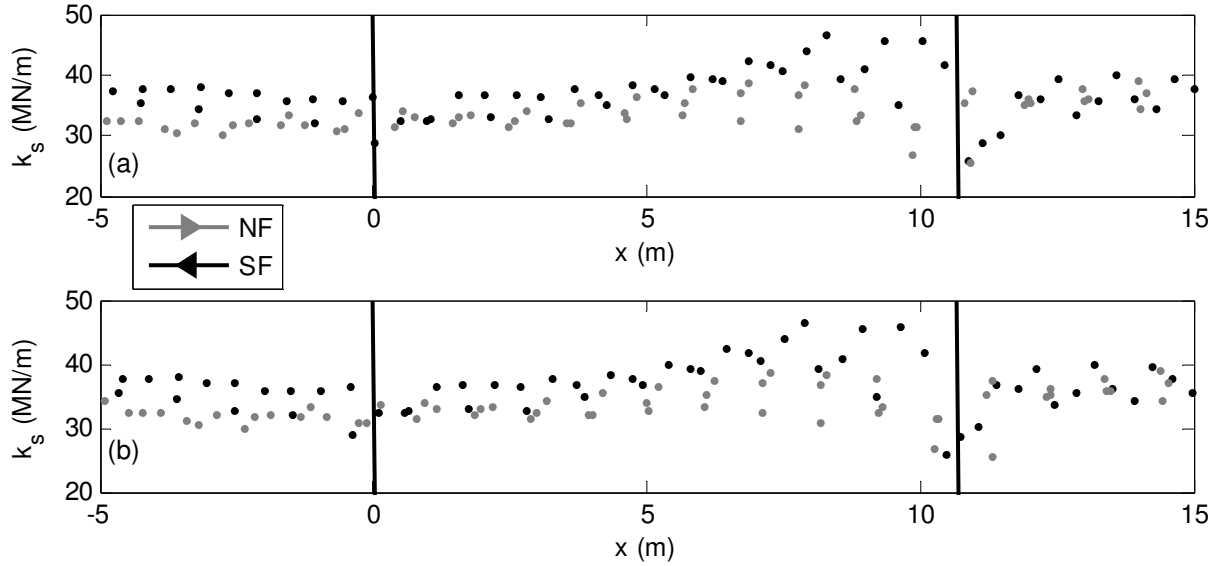

Figure B.2: Position error observed in k_s data records (TBFL18): (a) observed MV records with no correction; (b) MV position corrected by +0.40 m (1.3 ft)

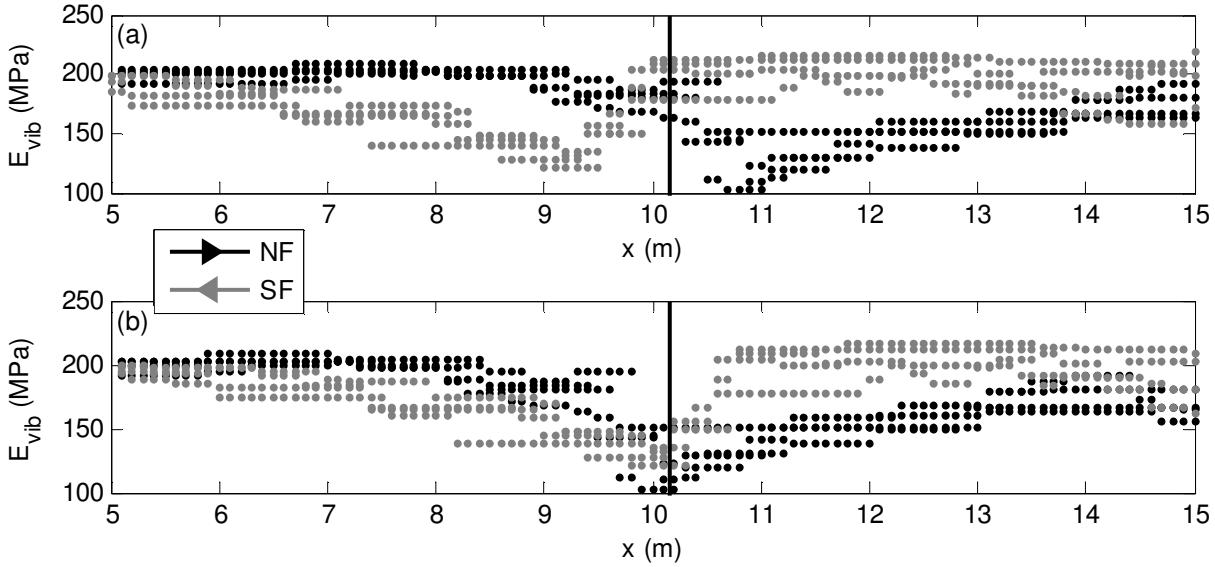

Figure B.3: Position error observed in E_{vib} data records (TBMD21): (a) observed MV records with no correction; (b) MV position corrected by -0.80 m (2.6 ft)

B.2 Repeatability of Roller MVs

Data from repeatability testing with the *CCV*, k_s, and E_{vib} MVs is presented here in Figures B.4 through B.6. Results are summarized in Chapter 3.

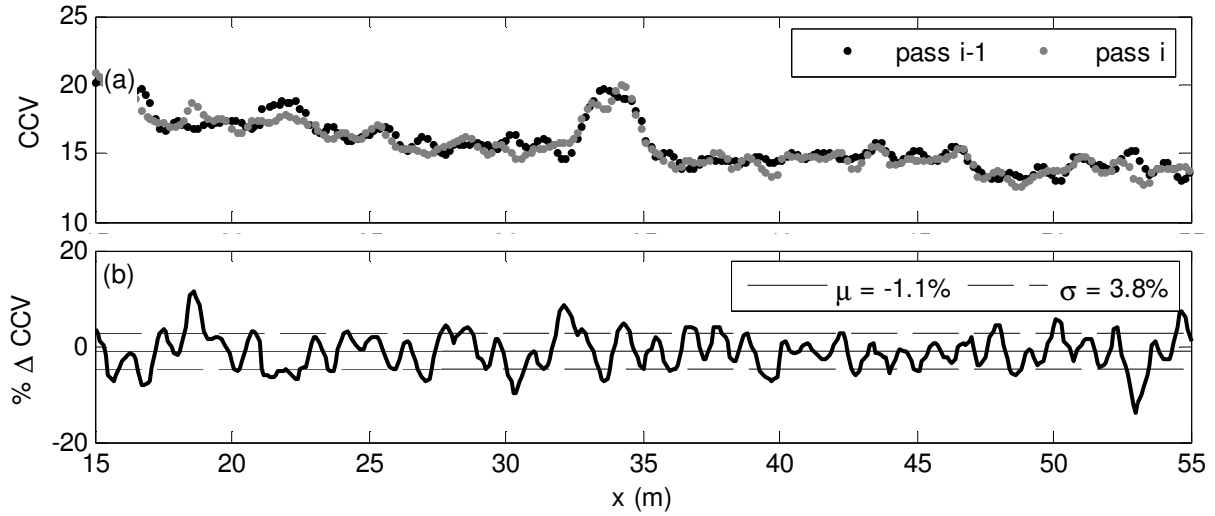

Figure B.4: Percent difference in CCV (smooth drum) determined via repeatability testing (TBFL18)

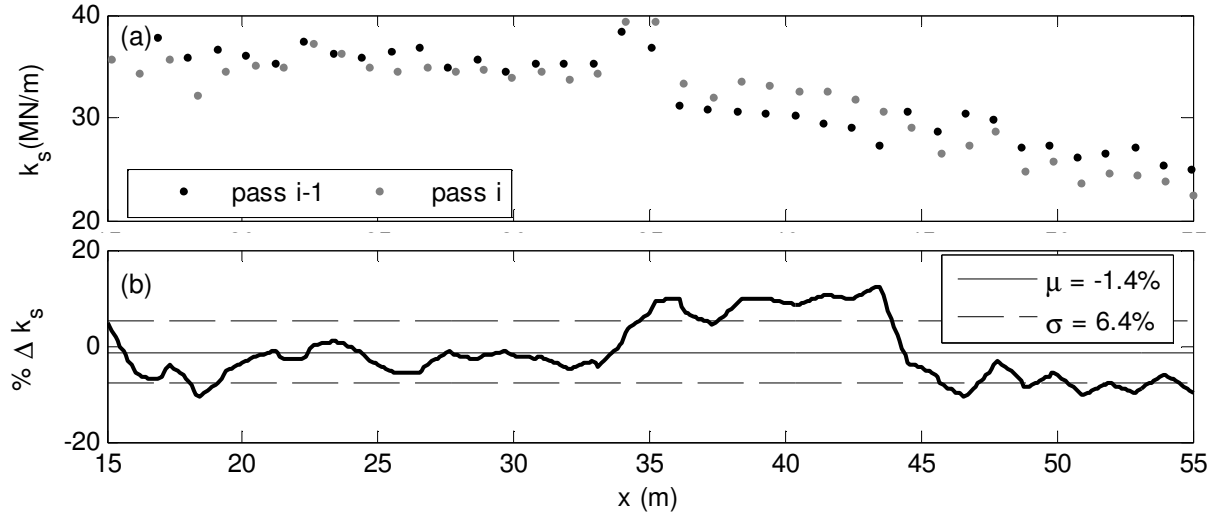

Figure B.5: Percent difference in k_s (smooth drum) determined via repeatability testing (TBFL18)

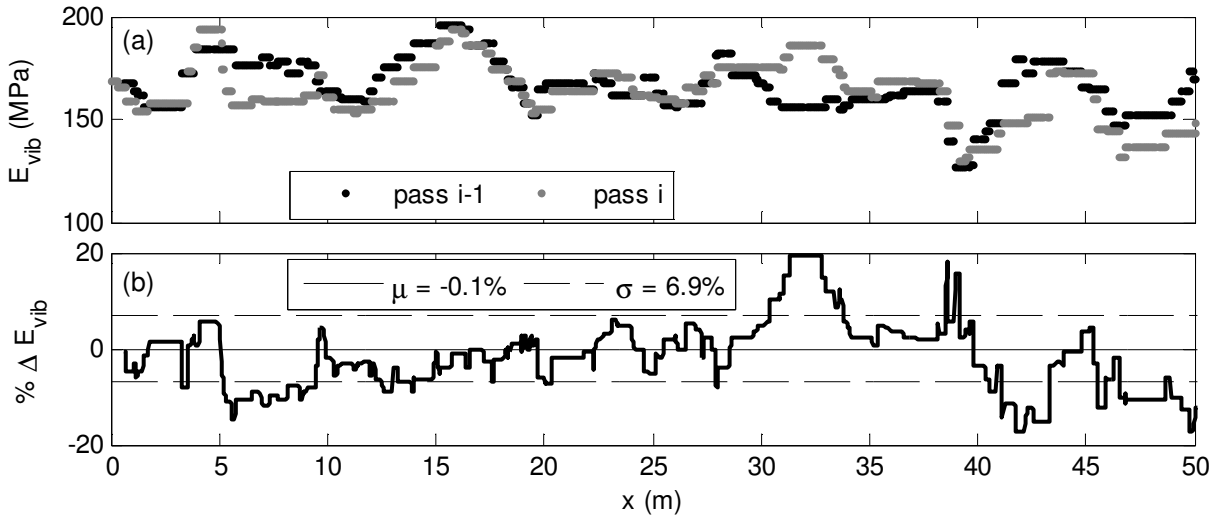

Figure B.6: Percent difference in E_{vib} (smooth drum) determined via repeatability testing (TBCO41)

B.3 Amplitude Dependence of Roller MVs

E_{vib} records from the Bomag smooth drum IC roller operated on TBMN42 are presented in Figure B.7. Five constant amplitude settings were used. For the low amplitude range, E_{vib} exhibited an increase in the x = 40-45 m region and a decrease in the x = 20-30 m region with increasing A. For this test bed, E_{vib} was found to be independent of A above 1.1 mm (0.043 in).

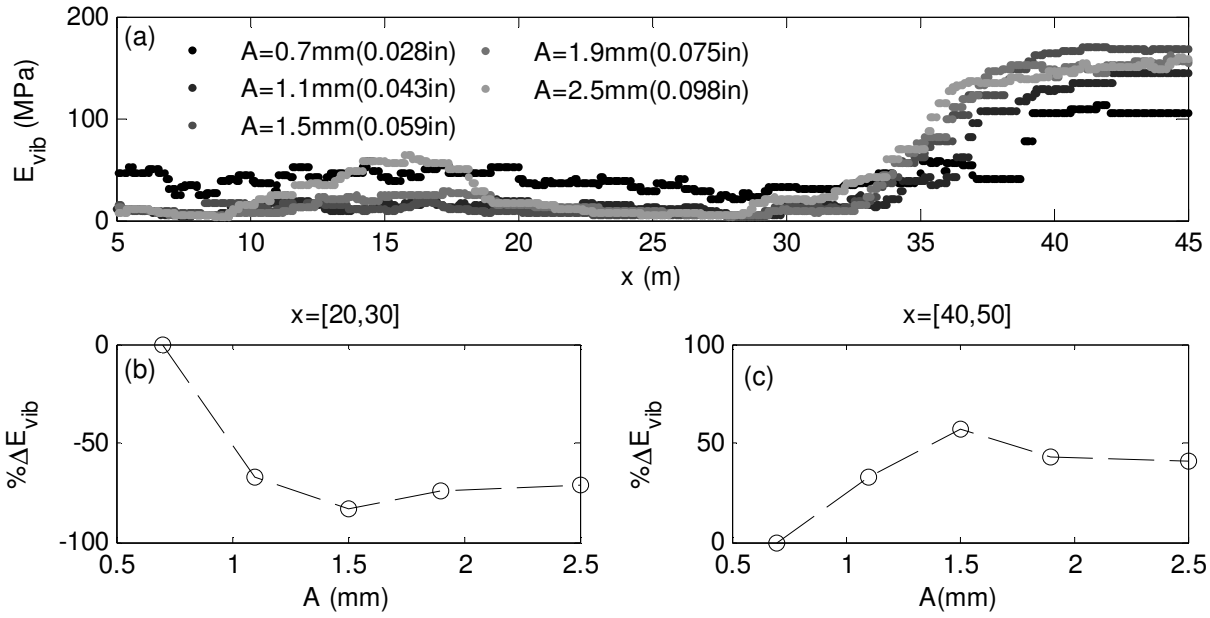

Figure B.7: Influence of A on E_{vib} (smooth drum) on granular and fine-grained material (TBMN42). Percent difference in mean roller MV shown for two regions in plots b and c.

Figure B.8 illustrates the influence of A on CCV, CCV_{CSM}, $k_{s\text{-}CSM}$ and CMV_{CSM} data collected or determined using the low and high amplitude settings of the Sakai CCC roller on granular subgrade material. The dependence of A on CCV is quite variable as shown in Figure B.8a, i.e., similar A = 0.8 mm (0.031 in) CCV data at x = 15 m and 30 m yield significantly different A = 2.1 mm (0.083 in) CCV data. The variability may be influenced by the previously documented insensitivity of CCV below 10. A similar observation holds for CMV_{CSM} data. Here, $k_{s\text{-}CSM}$ was reasonably similar for low and high amplitude vibration. A slight decrease in $k_{s\text{-}CSM}$ was observed at high amplitude. The discrepancy at x=33 m is due to jumping during high vibration.

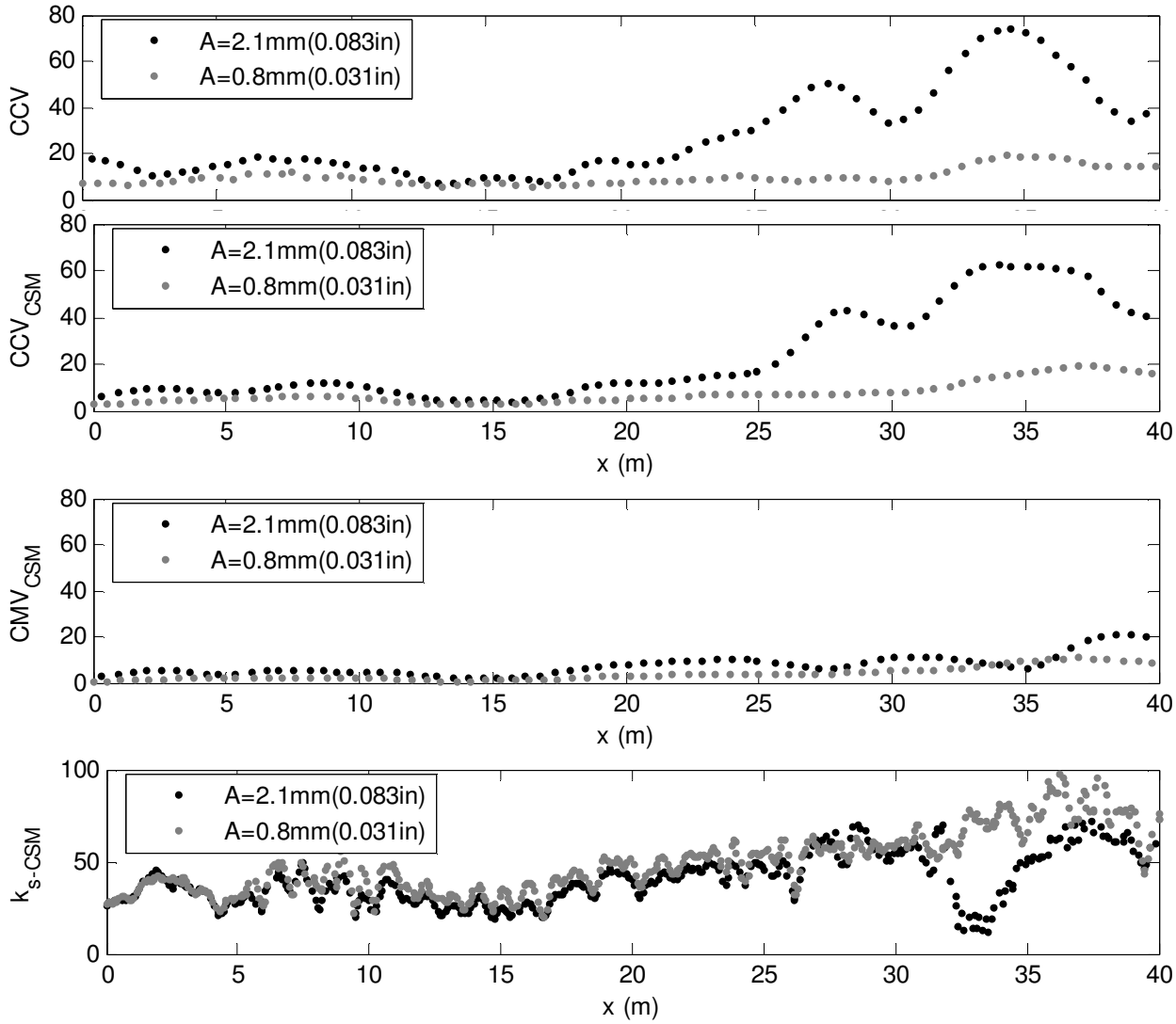

Figure B.8: Influence of A on roller MVs (smooth drum) on granular subgrade material (TBN 11)

The dependence of CMV_D on A was investigated using five centrifugal force amplitudes on granular subbase material. Figure B.9 shows the percent increase in CMV_D with increasing A. *CMV* is based on vibration harmonics manifested by partial loss of contact between the drum and soil. The degree of partial loss of contact is directly related to A, and therefore, *CMV* will be influenced by A. A similar principle applies for *CCV*.

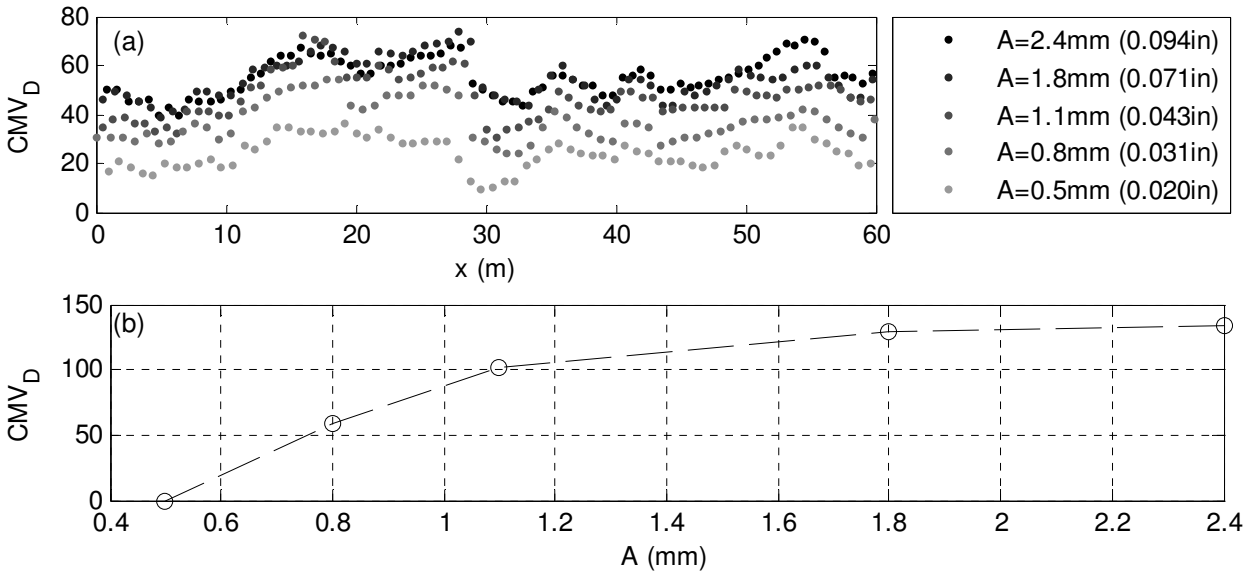

Figure 3.9: Influence of A on CMV_D (smooth drum) on granular and fine-grained material (TBCO33). Percent difference in mean roller MV shown in plot b

B.4 Forward Reverse Driving Direction Dependence of MVs

Bomag E_{vib} was found to decrease by 12% on average during reverse driving (see Fig. B.10). The Dynapac CMV_D did not exhibit any significant change during forward and reverse driving modes (see Fig. B.11). The mean percent change was 2.4 %. The Sakai *CCV* exhibited an 11% decrease in value during reverse driving (see Fig. B.12).

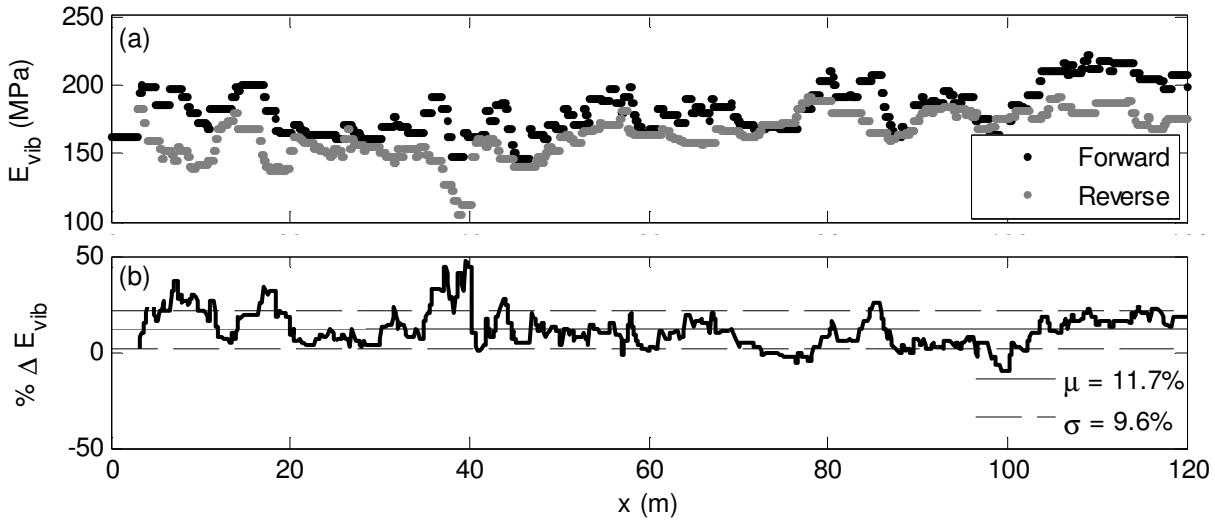

Figure B.10: Influence of forward-reverse driving mode on Bomag smooth drum E_{vib} (TBCO41). The percent difference (forward-reverse) is shown in plot b.

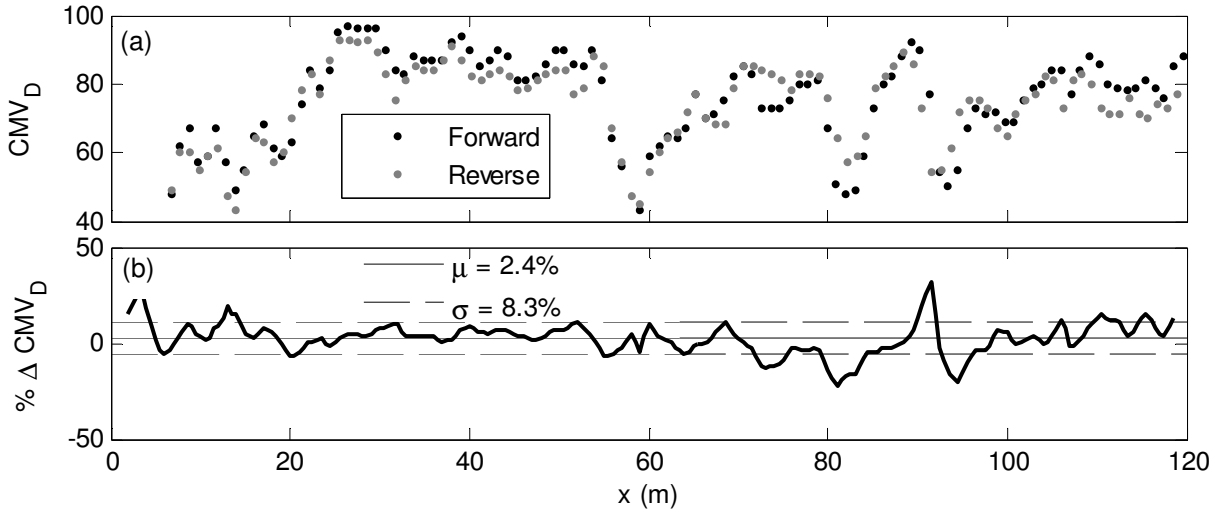

Figure B.11: Influence of forward-reverse mode on Dynapac smooth drum CMV_D (TBCO36). The percent difference (forward-reverse) is shown in plot b.

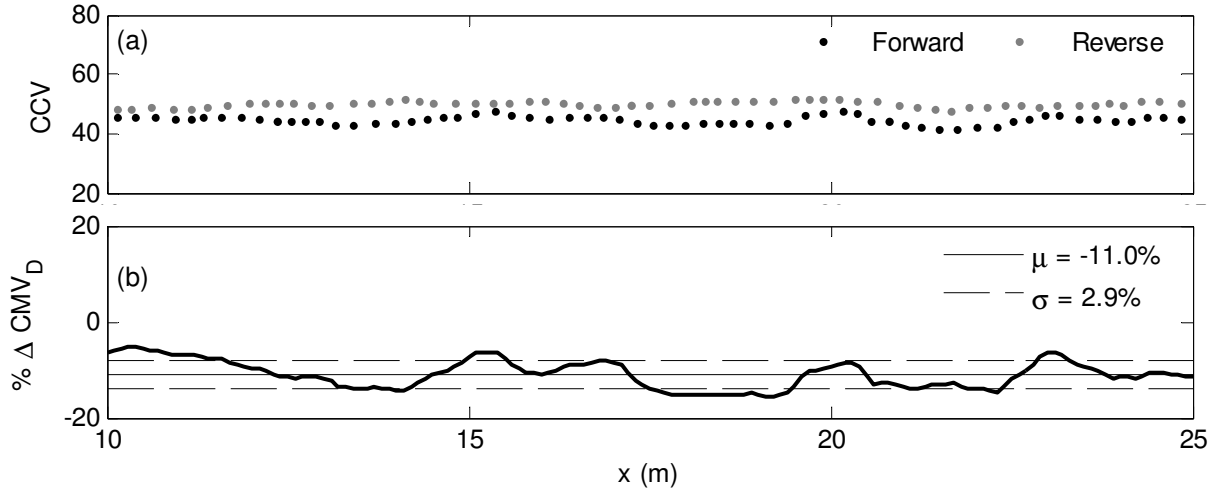

Figure B.12: Influence of forward-reverse mode on Sakai (record by CSM) smooth drum CCV (TBFL6) . The percent difference (forward-reverse) is shown in plot b.

B.5 Direction Dependence of Roller MVs

Figure B.13 illustrates the directional dependence of Sakai *CCV* and Case/Amman k_s on a heterogeneous single lane test bed (TBNC27). A directional difference in roller MV of 10% or more occurs on 70% of the test bed length. LWD tests were performed across the lane at three locations indicated by arrows in Figure B.13. Figure B.14 shows $E_{LWD\text{-}Z3}$ modulus versus the transverse position (y-axis) with superimposed roller MV data. The E_{lwd} profiles in Figures B.14a and b support the directional dependence observed in the k_s data. The E_{lwd} profile in Figure B.14c is relatively symmetric and serves to explain the equal MVs in both directions.

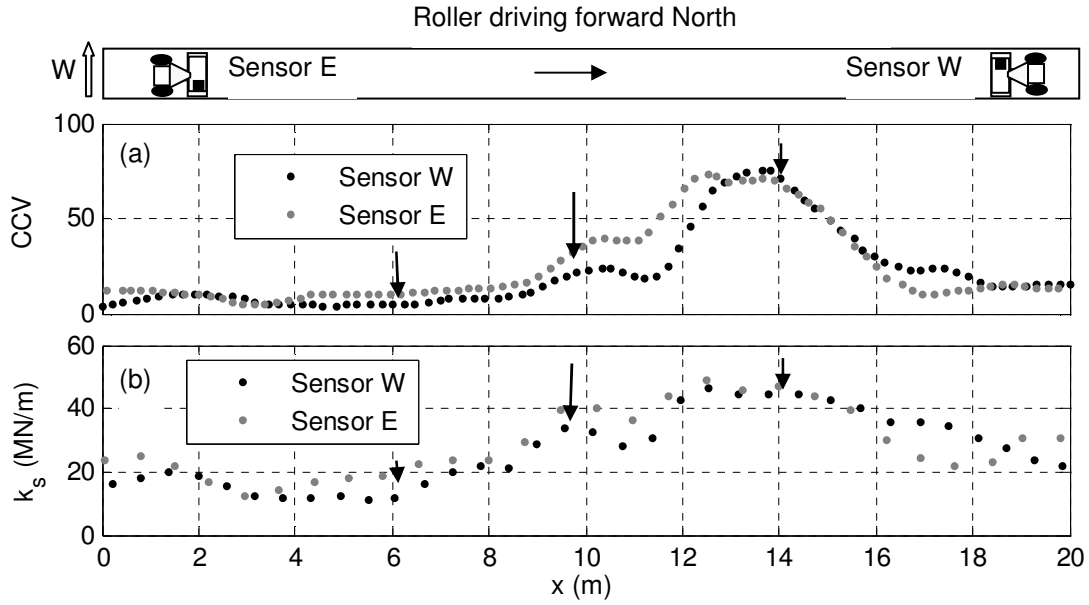

Figure B.13: Differences in directional roller MVs (TBNC27) due to transverse soil heterogeneity: a) Sakai roller CCV, and b) Case/ Ammann k_s data

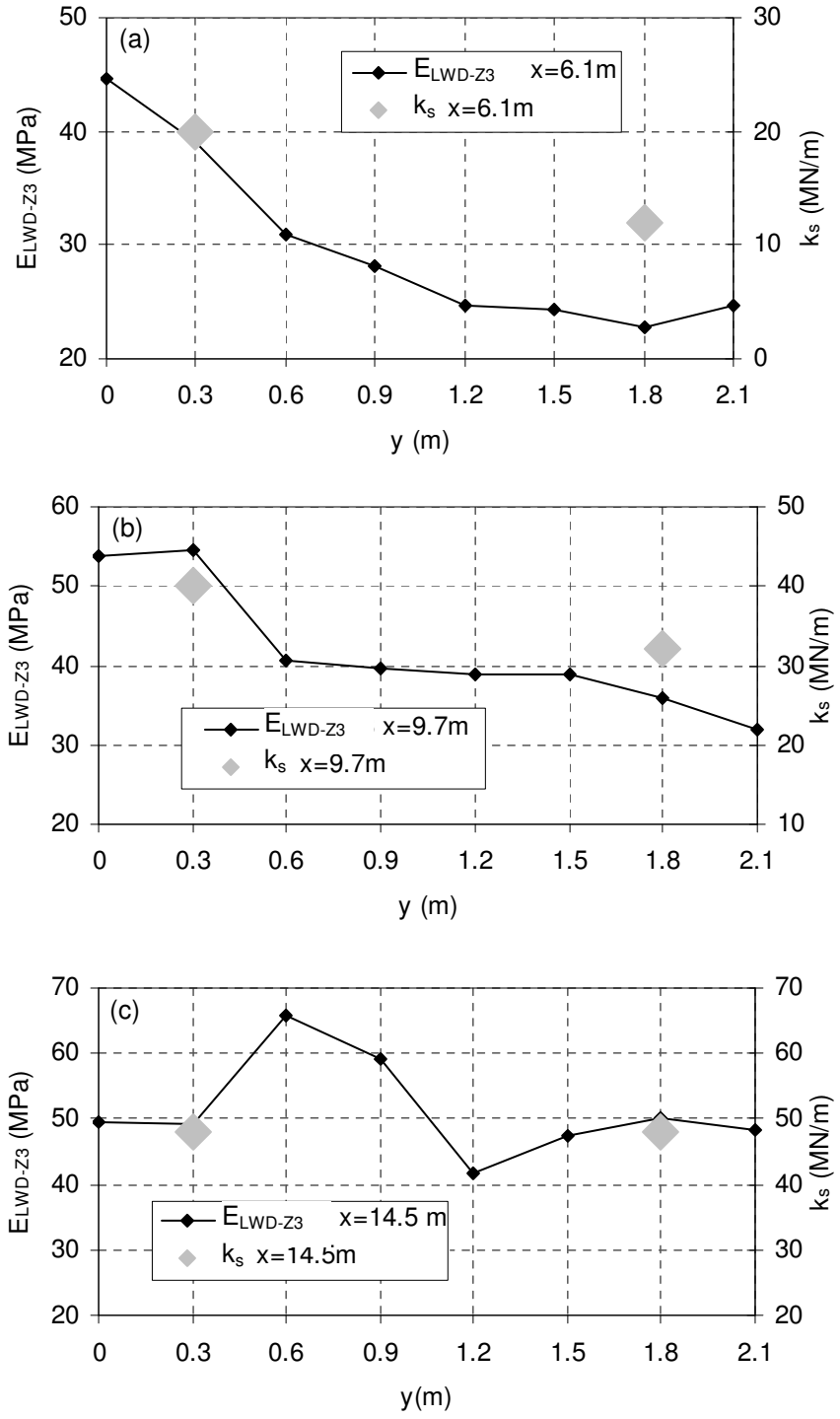

Figure B.14: Roller stiffness k_s and E_{LWD-Z3} variability across three lines (TBNC27)